Optimization of Sensitivity, Dose and Spatial Resolution in Edge Illumination X-Ray Phase-Contrast Imaging

Paul C. Diemoz, Marco Endrizzi, Charlotte K. Hagen, Fabio A. Vittoria, Thomas P. Millard, and Alessandro Olivo

***Abstract*–Edge illumination (EI) X-ray phase-contrast imaging has great potential for applications in a wide range of research, industrial and clinical fields. The optimization of the EI experimental setup for a given application is therefore essential, in order to take full advantage of the capabilities of the technique. In this work, we analyze the dependence of the angular sensitivity, spatial resolution and dose delivered to the sample upon the various experimental parameters, and describe possible strategies to optimize them. The obtained results will be important for the design of future EI experimental setups, in particular enabling their tailoring to specific applications.**

I. Introduction

OVER the two last decades, several X-ray phase-contrast imaging techniques (XPCi) have been developed and applied [1-7]. The increasing interest in this subject of research is motivated by the fact that these techniques, which measure the refraction/diffraction of the beam caused by the sample instead of its attenuation, can provide highly enhanced image contrast compared to conventional methods. However, their application has until now, with just few exceptions, been limited to synchrotron radiation (SR) facilities, due to the high spatial and temporal coherence usually required. The practical implementation with conventional sources would radically expand the range of applications of XPCi, by allowing its widespread use in research laboratories, in the industry and, ultimately, in clinical diagnostics.

The edge illumination (EI) XPCi method holds promise to solve most of the roadblocks encountered by other XPCi techniques. Originally developed as a synchrotron method [5], [8]-[9], it was later demonstrated to be efficiently applicable with laboratory sources [10]-[16]. This is primarily because EI is an intrinsically incoherent method, which does not exploit any wave interference/coherence effects, but only the purely geometrical refraction of the beam. In fact, its main principles can be explained by using simple ray-tracing optics, as shown in [17]. Therefore, EI is not affected by beam polychromaticity, and it provides intense signals even with sources featuring relatively large focal spots (up to at least 100 μm). Other advantages include robustness to mechanical vibrations, flexibility and scalability to large fields of view (required by many applications, notably in the biomedical field). Moreover, it was demonstrated that extremely high angular sensitivities of few nanoradians can be achieved using this method at SR facilities [9], and that sensitivities of EI laboratory setups are comparable to those obtained by other XPCi techniques, despite the simple setup [14].

In this work, we investigate the influence of various experimental parameters on the radiation dose delivered to the sample and on the two essential quantities describing the image quality: angular sensitivity and spatial resolution (the former determining the weakest refraction angle that can be detected in the image, while the latter determining the smallest detectable detail).

Manuscript received November 10, 2014. This work was supported by the UK Engineering and Physical Sciences Research Council (Grants EP/I021884/1 and EP/I022562/1). PCD and ME are supported by Marie Curie Career Integration Grants PCIG12-GA-2012-333990 and PCIG12-GA-2012-334056 within the Seventh Framework Programme of the European Union.

All authors are within the Department of Medical Physics and Bioengineering, University College London, Malet Place, Gower Street, WC1E 6BT London, UK (e-mail: p.diemoz@ucl.ac.uk).

II. The Edge Illumination Principle

The EI principle is based on illuminating the sample with a multitude of independent beamlets, created by means of an appropriate absorption mask (the so-called sample mask). The size of each beamlet ranges from few to tens of microns, depending on the particular implementation. A second mask (the detector mask), placed in contact with the detector, is used to analyze the radiation transmitted through the sample (see Fig. 1). It is slightly misaligned with respect to the first, so that a fraction of each beamlet is stopped by the mask, while the remaining part goes through the aperture and is counted by the detector. When a sample is introduced, each beamlet is not only reduced in intensity due to attenuation in the sample, but also deflected due to refraction. The latter effect can either increase or decrease the number of counts on the detector, according to the direction of refraction. This leads to the creation of black or white fringes in the image, highlighting the boundaries of the various object structures, where the refraction is highest.

If the object transmission is denoted with $T(y)$, and the refraction angle along the direction y orthogonal to the apertures with $\Delta\theta_y(y)$, the signal recorded by each detector pixel can be expressed as [9], [14]:

$$S(y) = N \cdot T(y) C\left(y_e - z_2 \cdot \Delta\theta_y(y)\right) \quad (1)$$

where N is the number of photons in each beamlet, z_2 is the distance between the sample and the second mask, y_e is the

misalignment between the two masks and $C(y_e)$ is the so-called illumination curve. This expresses the fraction of photons transmitted through the second mask, as a function of the masks misalignment. $C(y_e)$ is comprised between a value close to 1 (when the masks are perfectly aligned) and a value close to 0 (when they are completely misaligned, so that the beam produced by the first mask impinges on the absorbing part of the second).

EI acquisitions are often performed using a 50% illumination condition, which is achieved when the edge of the detector slit is aligned with the centre of the sample slit (see Fig. 1). This leads to half of the beam being stopped, and half going through to the detector. The refraction-induced spatial shift of the beam, which is equal to $z_2 \cdot \Delta\theta_y(y)$ at the detector plane, has the effect of changing the percentage of photons going through the second aperture, therefore producing image contrast.

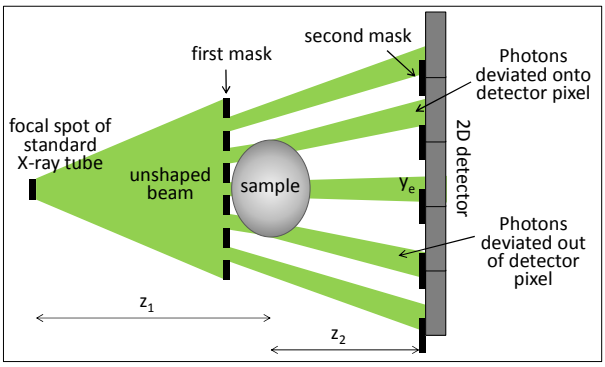

Fig. 1. Scheme of the edge illumination setup (not to scale). Each slit is assumed to extend along the direction *x* orthogonal to the plane of drawing, in order to illuminate a line of detector pixels along *x*.

The EI image contains, in the general case, a mixture of attenuation and refraction contrast, as seen from (1). Phase retrieval algorithms that enable disentangling and evaluating these two object quantities have been developed [9], [11], [14]. These are based on acquiring two images of the same sample at complementary mask positions $y_{e,\pm}$ (with the detector mask chopping either the lower or the upper part of the beam). The object transmission and refraction angle functions can then be calculated as [14]:

$$T(y) = \frac{S_+(y)}{N \cdot C\left[y_{e,+} - R^{-1}\left(\frac{S_+(y)}{S_-(y)} \right) \right]} \qquad (2)$$

$$\Delta\theta_y(y) = -\frac{1}{z_2} R^{-1}\left(\frac{S_+(y)}{S_-(y)} \right) \qquad (3)$$

where S_+ and S_- are the images acquired in the two complementary positions, and the auxiliary function R is defined as:

$$R(z_2\Delta\theta_y) \equiv \frac{C(y_{e,+} - z_2\Delta\theta_y)}{C(y_{e,-} - z_2\Delta\theta_y)} \qquad (4)$$

The function R can be easily calculated from the experimental measure of the illumination curve, which is obtained by scanning one mask with respect to the other and recording the detector intensity at each point of the scan.

III. Setup Optimization

In order to take full advantage of the capabilities of EI for a given application, the optimization of the experimental setup is of central importance. In particular, two quantities defining the image quality need to be considered: the angular sensitivity and the spatial resolution.

We define the angular sensitivity as the smallest refraction angle detectable by a given setup. By propagating the noise in the two input images S_+ and S_- (assumed to be of purely stochastic origin) through (3), it can be found that the uncertainty on the calculated refraction angle is equal to [14]:

$$\alpha = \sigma(\Delta\theta_y) = \frac{\sqrt{C(y_e)}}{z_2\sqrt{2TN}\left[\rho_{ref}(y_e) - \rho_{ref}(y_e + d)\right]} \qquad (5)$$

where d is the size of each detector aperture and ρ_{ref} is the beam spatial distribution on the detector plane. The noise in the refraction image is a direct indicator of the smallest detectable refraction angle. Only angles that are larger than the background noise, in fact, can be effectively detected in the image.

Equation (5) offers a simple and practical way to estimate the sensitivity of a given existing setup, or to guide the design of a new one. Apart from the trivial dependence on the number of photons (which determines the statistics and therefore the image noise), we see that the sensitivity depends on the setup geometry, and can therefore be optimized by varying the relevant experimental quantities. These include the propagation distance, the misalignment between the masks and the spatial distribution of the beam on the detector plane (which depends, in turn, on the setup distances and the size of the aperture of the first mask).

In addition to maximizing the sensitivity, however, in several applications it is important to reduce the radiation dose delivered to the sample. This is the case for small animal imaging and for clinical applications, where the dose should be kept as low as possible and typically below pre-determined limits. The dose is proportional to the photon density, i.e. $D = K_{dose} \cdot N/p$, where p is the period of the sample mask and K_{dose} is a constant depending in a complex way on the photon energy and on the shape and composition of the sample. A useful figure-of-merit to describe the sensitivity of a given setup at a fixed dose is represented, in this case, by the quantity $\alpha \cdot \sqrt{D}$, which is independent of the flux of photons on the sample [18], [19]. Note that, in other applications (such as industrial non-destructive testing, materials science, the

study of dynamical processes, etc.), it may be more important to minimize the acquisition time and therefore define a different figure-of-merit such as $\alpha\cdot\sqrt{t}$. Note that the number of photons is related to the exposure time through the relation $N = f\cdot a\cdot t$, where f is the photon flux on the sample mask, i.e. the number of photons per unit of length and unit of time. In the following examples, we will show that this can lead to different values for the optimal setup parameters, compared to an optimization with respect to the dose.

Another essential quantity to consider is spatial resolution, which is also influenced by the setup geometry. We found in previous work that, under the geometrical approximation (which was demonstrated to be valid for laboratory setups based on non-microfocal sources [17], [20]), the point spread function for the refraction signal is equal to [17], [21]:

$$PSF = \left[g\left(y - y_e/M\right) - g\left(y - y_e/M - d/M\right)\right]\cdot rect\left(y + a/2\right) \tag{6}$$

where the function g indicates the source intensity distribution projected onto the detector plane, $M = \left(z_1 + z_2\right)/z_1$ is the geometrical magnification, z_1 is the source-to-sample distance, and a is the size of the apertures in the first mask. $rect_a\left(y + a/2\right)$ is a rectangular function, equal to 1 in the range (0, a) and 0 elsewhere, which represents an aperture in the first mask. In the above equation, we have assumed that dithering (i.e. sub-pixel scanning of the sample along y, a procedure typically used to improve the spatial resolution [21],[22]) is performed, and that the scan step is small compared to the masks period. Therefore, the calculated PSF represents the maximum spatial resolution achievable by the imaging system (without dithering, in fact, the resolution would be simply equal to the period of the sample mask). Note that, if dithering is carried out, both the dose and the exposure time increase proportionally to the total number of dithering steps, i.e. the improved spatial resolution comes at the price of a larger dose to the sample and a longer time needed for the acquisition.

Equation (6) can be used as the basis for an optimization of the parameters aimed at maximizing the spatial resolution. In the following example, we show that this leads to different optimal acquisition conditions compared to an optimization with respect to the angular sensitivity. We consider here the experimental parameters of one of the laboratory setups available at University College London. The source is a Rigaku M007 Mo, operated at 35 kV and featuring a source full width at half maximum (FWHM) of 70 µm. The detector is an ANRAD "SMAM" amorphous selenium flat panel, with a pixel size of 85 µm. The considered distances are z_1 = 1.6 m and z_2 = 0.4 m, the detector aperture is d = 20 µm and a 50% illumination is considered. The width of the PSF, and the quantities $\alpha\cdot\sqrt{D}$ and $\alpha\cdot\sqrt{t}$, are calculated as a function of the aperture size a, which is left as the free parameter to be optimized (Fig. 2).

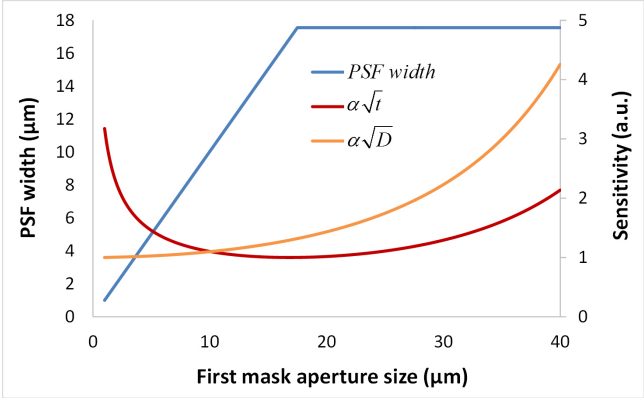

Fig. 2. Optimization of sensitivity and spatial resolution as a function of the size of the first mask aperture.

For large apertures, the achievable spatial resolution is only determined by the source blurring, while for small apertures it is limited by the aperture size itself. This is due to the fact that regions of the sample that are covered by the mask are not illuminated, and therefore cannot contribute to the image signal. The fact that the aperture size limits the extent of the PSF width (see (6) and Fig. 2) provides a very interesting possibility to achieve microscopic resolutions even with extended sources and large pixels. The quantity $\alpha\cdot\sqrt{D}$ is also optimized at small values of the parameter a, as the sensitivity at a fixed dose to the sample is maximized in this case. However, the quantity $\alpha\cdot\sqrt{t}$ has a very different trend, having a minimum at about 16.8 µm. Large mask apertures, in fact, lead to a wider beam distribution onto the detector (thus reducing the sensitivity), while small apertures reduce the photon flux (thus increasing the image noise at a fixed time, or equivalently the time needed to achieve a given signal-to-noise ratio). Note that $\alpha\cdot\sqrt{D}$ is not so sensitive to the latter effect, because this is also accompanied by a reduction of the dose to the sample. We have thus shown that trade-offs exist between minimization of dose and of time, and between sensitivity and achievable spatial resolution, which means that improving one of the two inevitably leads to a compromise on the other one.

The second example deals with the important practical case where the sensitivity needs to optimized with respect to masks misalignment. Here, the sample aperture is assumed to be a = 12 µm (like in our experimental setup), while the other parameters are the same as in the first example. The quantity $\alpha\cdot\sqrt{D}$ is reported in Fig. 3, as a function of the parameter y_e. Contrary to the previous example, $\alpha\cdot\sqrt{D}$ and $\alpha\cdot\sqrt{t}$ share the same value for the optimal misalignment y_e. In fact, $D/t = f\cdot a/p\cdot K_{dose}$ does not depend on this parameter, thus the two curves only differ by a constant factor.

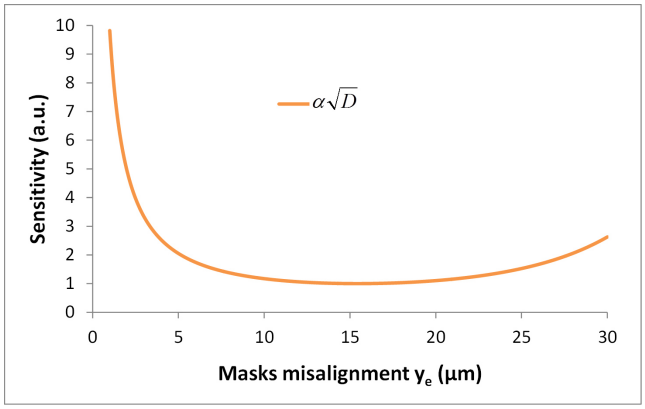

Fig. 3. Optimization of the sensitivity as a function of the misalignment between the two masks.

It can be seen from Fig. 3 that $\alpha \cdot \sqrt{D}$ is minimum (corresponding to highest sensitivity for a given radiation dose to the sample) at y_e = 15.4 µm. A smaller misalignment, corresponding to a higher illumination condition, would lead to smaller contrast (i.e. lower relative change in signal with the sample in the beam compared to the reference case without sample). However, larger misalignment would lead to a lower number of photons being detected, thus increasing the image noise.

IV. Conclusions

In this work, we have derived analytical expressions relating the achievable angular sensitivity and spatial resolution of an EI imaging system to the various experimental parameters. These expressions enable the optimization of the experimental setup on the basis of the type of samples that have to be imaged, the structures to be visualized, their size, etc. and constraints such as radiation dose and acquisition time.

We have suggested and discussed possible optimization strategies. In particular, we showed that a trade-off exists, like in other XPCi techniques, between spatial resolution and angular sensitivity. Moreover, the optimization of sensitivity with respect to either the acquisition time or the radiation dose to the sample provides in general different values for the optimal parameters. We believe that the results of this analysis will be an extremely useful guide for the design of future experimental setups based on the EI principle.

References

[1] S. W. Wilkins *et al.*, "On the evolution and relative merits of hard X-ray phase-contrast imaging methods", Phil. Trans. R. Soc. A, vol. 372, no. 20130021, 2014.

[2] A. Snigirev, I. Snigireva, V. Kohn, S. Kuznetsov, and I. Schelokov, "On the possibility of X-ray phase contrast microimaging by coherent high-energy synchrotron radiation", Rev. Sci. Instrum., vol. 66, issue 12, pp. 5486-5492, 1995.

[3] T. Davis, D. Gao, T. E. Gureyev, A. W. Stevenson, and S. W. Wilkins, "Phase-contrast imaging of weakly absorbing materials using hard X-rays", Nature, vol. 373, issue 6515, pp. 595–598, 1995.

[4] A. Momose T. Takeda, Y. Itai and K. Hirano, "Phase-contrast X-ray computed tomography for observing biological soft tissues", Nat. Med., vol. 2, pp. 473-475, 1996.

[5] A. Olivo *et al.*, "An innovative digital imaging set-up allowing a low-dose approach to phase contrast applications in the medical field", Med. Phys., vol. 28, issue 8, pp. 1610-1619, 2001.

[6] A. Momose et al., "Demonstration of X-ray Talbot interferometry", Jpn. J. Appl. Phys., vol. 42, L866–L868, 2003.

[7] F. Pfeiffer, T. Weitkamp, O. Bunk, and C. David, "Phase retrieval and differential phase-contrast imaging with low-brilliance X-ray sources", Nat. Phys., vol. 2, issue 4, pp. 258-261, 2006.

[8] A. Olivo, P. C. Diemoz, and A. Bravin, "Amplification of the phase contrast signal at very high X-ray energies", Opt. Letters, vol. 37, issue 5, pp. 915-917, 2012.

[9] P. C. Diemoz *et al.*, "X-ray phase-contrast imaging with nanoradian angular resolution", Phys. Rev. Lett., vol. 110, issue 13, no. 138105, 2013.

[10] A. Olivo and R. D. Speller, "A coded-aperture technique allowing X-ray phase contrast imaging with conventional sources", Appl. Phys. Lett., vol. 91, no. 074106, 2007.

[11] P. R. T. Munro, K. Ignatyev, R. D. Speller, and A. Olivo, "Phase and absorption retrieval using incoherent X-ray sources", Proc. Natl. Acad. Sci. USA, vol. 109, no. 13922, 2012.

[12] M. Marenzana *et al.*, "Visualization of small lesions in rat cartilage by means of laboratory-based x-ray phase contrast imaging", Phys. Med. Biol., vol. 57, issue 24, pp. 8173–8184, 2012.

[13] A. Olivo *et al.*, "Low-dose phase contrast mammography with conventional X-ray sources," Med. Phys., vol. 40, issue 9, no. 090701, 2013.

[14] P. C. Diemoz, C. K. Hagen, M. Endrizzi, and A. Olivo, "Sensitivity of laboratory based implementations of edge illumination X-ray phase-contrast imaging", Appl. Phys. Lett., vol. 103, no. 244104, 2013.

[15] M. Endrizzi *et al.*, "Hard X-ray dark-field imaging with incoherent sample illumination", Appl. Phys. Lett., vol. 104, no. 024106, 2014.

[16] C. K. Hagen, P. R. T. Munro, M. Endrizzi, P. C. Diemoz and A. Olivo, Med. Phys., vol. 41, no. 070701, 2014.

[17] P. C. Diemoz and A. Olivo, "On the origin of contrast in edge illumination X-ray phase-contrast imaging", Opt. Express, to be published.

[18] P. C. Diemoz, A. Bravin, and P. Coan, "Theoretical comparison of three X-ray phase-contrast imaging techniques: propagation-based imaging, analyzer-based imaging and grating interferometry", Opt. Express, vol. 20, pp. 2789-2805, 2012.

[19] P. C. Diemoz, M. Endrizzi, A. Bravin, I. K. Robinson, and A. Olivo, "Sensitivity of edge illumination X-ray phase-contrast imaging", Phil. Trans. R. Soc. A, vol. 372, no. 20130128, 2014.

[20] P. R. T. Munro, K. Ignatyev, R. D. Speller, and A. Olivo, "The relationship between wave and geometrical optics models of coded aperture type X-ray phase contrast imaging systems", Opt. Express, vol. 18, issue 5, pp. 4103-4117, 2010.

[21] P. C. Diemoz, F. A. Vittoria, and A. Olivo, "Spatial resolution of edge illumination X-ray phase-contrast imaging", Opt. Express, vol. 22, issue 13, pp. 15514-15529, 2014.

[22] K. Ignatyev, P. R. T. Munro, R. D. Speller, and A. Olivo, "Effects of signal diffusion on X-ray phase contrast images," Rev. Sci. Instrum., vol. 82, issue 7, no. 073702, 2011.